Sea surface temperature of oceans surrounding subequatorial Africa: seasonal patterns, spatial coherence and long-term trends

C.A. Villacastín-Herrero*[1], L.G. Underhill[2], R.J.M. Crawford[3] and L.V. Shannon[3†]

[1]Marine Biology Research Institute, Zoology Department, University of Cape Town, Rondebosch, 7700 South Africa; [2]Department of Statistical Sciences, University of Cape Town; [3]Sea Fisheries Research Institute, Private Bag X2, Rogge Bay.

A Fourier-type regression equation is used to model monthly values and long-term temporal trends of sea surface temperature (SST) in 88 areas of the South Atlantic and South Indian oceans surrounding subequatorial Africa, based on more than two million measurements of SST over a period of 81 years (1910–1990). In most of the 81 areas north of 40°S, the model accounts for a large portion of the observed variance in SST records and predicts well-defined seasonal trends in SST. In the more southerly areas (between 20° and 40°S), the peak in SST occurs in February, closer to the Equator it occurs in March, and in some areas near the Equator influenced by the South Equatorial Current in April. In most of the Indian Ocean considered, around the African coast and immediately south of the Equator in the Atlantic Ocean, the minimum SST is in August. Elsewhere in that portion of the Atlantic Ocean investigated it is in September. High seasonal amplitudes in SST occur near the African coast in regions influenced by the Angola and Agulhas currents and in the central South Atlantic where isotherms migrate meridionally. Coherence in SST residuals between modelled results and observed data indicates that several large regions of the ocean are influenced similarly. These regions generally conform with known oceanographic features. The coastal regions off western South Africa show affinities with several ocean areas and because of the influence of several oceanographic regimes are likely to be highly variable. The model suggests an average warming of 0.46°C in the region between 1910 and 1990.

The marine environment around southern Africa is highly variable, being influenced both by local events and by intrusions of water from farther afield.[1] For example, the shelf off western southern Africa may be influenced by input of water from the north, the east and the south.[1–3] The variability of the marine environment has important consequences for the fish populations, and other living resources, of the region.[4,5]

Preliminary analyses have indicated that perturbations in the coastal waters off southern Africa are linked with environmental changes in the North Atlantic Ocean,[6] and that changes in the distributions and abundances of organisms in the Benguela system similarly may be linked to changes in the biota of the North Atlantic, and even in some systems of the Pacific Ocean.[6–9]

McLain *et al.*,[10] in a comprehensive study of sea surface temperatures within the Benguela, found that SST anomalies were more persistant through time rather than with distance. Walker[11] suggested that ocean dynamics and atmospheric forcing within the South-East Atlantic region should encompass a larger portion of the basin to allow for possible associations between SST and local atmospheric forcing. The basin-wide spatially arranged effects within the Benguela have been further evidenced by Brundrit,[12] who found good correlation between nearshore SST and sea-level trends.

This paper further explores the possibility of linkages in the marine environment over large spatial scales by investigating relationships between records of sea surface temperature in areas of 5° latitude and 5° longitude or, where data are sparse, combinations of such areas. The region considered is that surrounding subequatorial Africa, from the Equator to 50°S, and from 25°W to 50°E (Fig. 1).

Material

For all areas, SST records archived by the South African Data Centre for Oceanography (SADCO) were used in the analysis. SST data at SADCO are mainly those taken by merchant Voluntary Observing Ships (VOS) and by ships of opportunity, collated at the Meteorological Office in the UK. They provide the longest available time series of surface oceanic measurements around southern Africa. For some areas data were augmented with information obtained from SST charts compiled by the Maritime Office of the South African Weather Bureau and from Bruce.[13]

SST data for the period 1910–1990 (see Table 1) were used, as in these years there were usually more than five monthly records for most 5 × 5° areas. In earlier years there was a scarcity of SST records. Total numbers of SST observations used for each 5 × 5° area, or combination of areas, are listed in Table 1. The entire study area had more than two million records for the period investigated. Data density was high in the main commercial shipping lanes and around the coast, whereas in the deep ocean and at southern latitudes there were considerably fewer measurements. Numbers of SST records in each year are shown for three areas (chosen from the three main oceanic areas) in Fig. 2. There is substantial variation between months in the number of records available. Few data were collected during World War II (1939–45), whereas there were many observations in the 1970s and 1980s.

As SST records in the SADCO database had not been checked, they were screened for outliers by visually inspecting box-whisker plots of the data. Records were deleted if they deviated from those in the same 5 × 5° area for the same month in that year and in the three preceding and three succeeding years by more than two standard deviations. Biases in SST records result from changes in non-climatic factors such as methods of measuring temperature (canvas buckets, subject to evaporative cooling, were typically used prior to 1945 and engine intakes thereafter),[14] ships used to measure SST (including the conversion from sail to steam and trends in ship size) and shipping routes.[15–17] Corrections to account for these biases were made from information in Jones *et al.*,[18] who used a database of over 63 million records to compare trends in SST records in the Southern Hemisphere with land air temperatures. SST values

*Author for correspondence. Present address: Marine Environment Unit, Institute for Remote Sensing Applications, Joint Research Centre, European Commission, Ispra (Va), I-21020, Italy. E-mail: carlos.villacastin@jrc.it.
†Present address: Dept. of Oceanography, University of Cape Town.

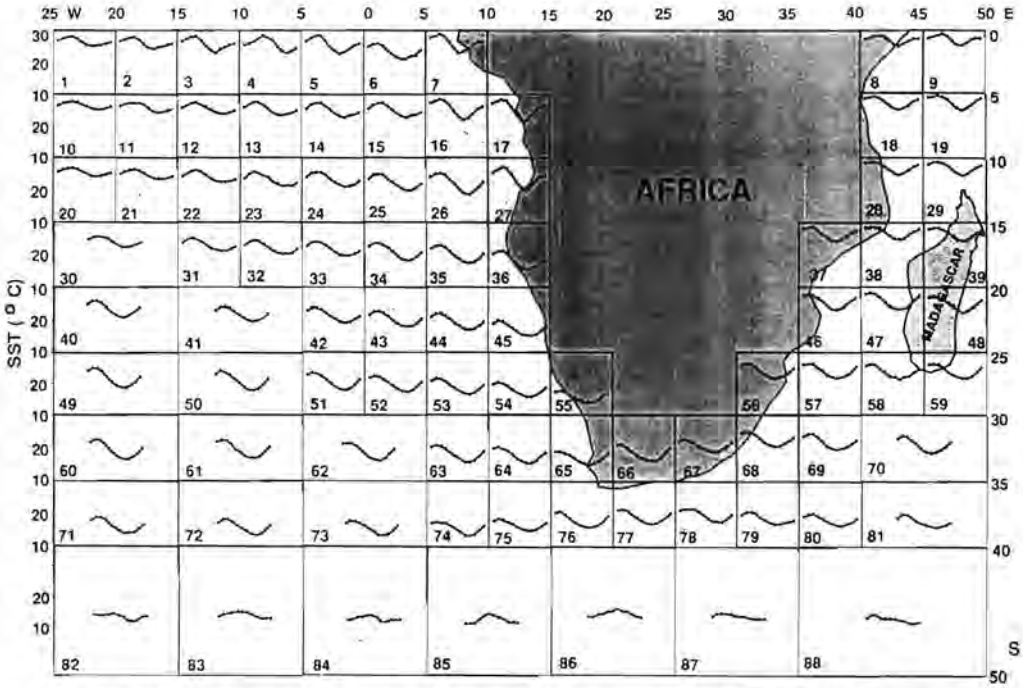

Fig. 1. The 88 areas considered in the analysis, showing the values of SST for each month computed by the Fourier model (commencing January, ending December).

between 1903 and 1940 were increased by 0.49°C. Those in 1941 were increased by 0.19°C. Records between 1942 and 1945 were reduced by 0.1°C. These corrections are in accord with factors employed by Folland *et al.*[19] Although the quality control applied to the data is by no means exhaustive, it was believed to be reasonable in view of the nature of the statistical analysis in use here.

Table 1. Numbers of SST records for each of the areas used in the analysis, 1910–1990. Area numbers refer to those used in Fig. 1.

1	9508	23	12595	45	37995	67	96035
2	10931	24	72056	46	77415	68	60726
3	9592	25	83713	47	7220	69	21060
4	144915	26	10368	48	16250	70	22174
5	52963	27	11987	49	10999	71	3282
6	15659	28	46777	50	7386	72	5237
7	25464	29	12925	51	7643	73	6840
8	26141	30	11300	52	51115	74	7617
9	29051	31	12136	53	23473	75	8543
10	8168	32	10852	54	163979	76	14570
11	8457	33	17583	55	32176	77	21356
12	12187	34	61689	56	79710	78	9027
13	35164	35	80163	57	50065	79	7340
14	129501	36	32274	58	42947	80	6218
15	12153	37	33851	59	33658	81	10879
16	12354	38	47820	60	10608	82	1652
17	11449	39	2143	61	11704	83	1816
18	25459	40	4268	62	19347	84	2624
19	20540	41	14535	63	17642	85	6806
20	12880	42	14613	64	77247	86	2732
21	11072	43	50793	65	246627	87	3733
22	9556	44	135475	66	99948	88	12397

Methods

For each month in each year and area, the mean and standard deviation of SST, as well as the minimum and maximum, were determined. This allowed us to identify the clear outliers. A multiple regression model was used to describe seasonal patterns of SST in each block. The dependent variable was Y_t, the mean of all available SSTs in month t, where t is measured in months since January 1910. The functional form of the model was:

$$Y_t = a + bt + c_1 \sin\theta_t + d_1 \cos\theta_t + c_2 \sin 2\theta_t + d_2 \cos 2\theta_t + e \qquad (1)$$

where a, b, c_1, c_2, d_1 and d_2 are regression coefficients estimated by the method of least squares; θ_t, in degrees, represents the midpoint of the month of the year in which the observation Y_t was made; and e represents the residuals, assumed to have a normal distribution with mean 0 and variance σ^2. The term bt in the regression model enables us to test for long-term trend in SST. The trigonometric terms enable us to model the annual seasonality in SST. Thus the value of θ_t for observations made in January of any year is 15°, for February is 45°, ... for December is 345°. The inclusion of the terms for second harmonics ($\sin 2\theta_t$ and $\cos 2\theta_t$) improves the flexibility of the model in fitting the seasonality. Higher order harmonics were tried but not required. Similar models for seasonality have described rainfall probabilities[20] and the occurrence of migrant birds.[21]

The Fourier-type model with trigonometric terms, as in Equation (1), holds an advantage over the more standard approach of computing the mean SST for each month, because fewer parameters are required to describe the seasonal pattern. Here, we use four parameters rather than 12 to describe seasonality. In addition, the regression method enables the fitting of a term to take account of long-term temporal trends, and the regression coefficient b in (1) represents the average monthly linear trend in SST.

Monthly anomalies were computed as the residuals from the fitted model (1). These residuals were used to compute 'distances' between two areas, i and j say. Let e_{it} be the difference between the observed and fitted values in block i in month t.

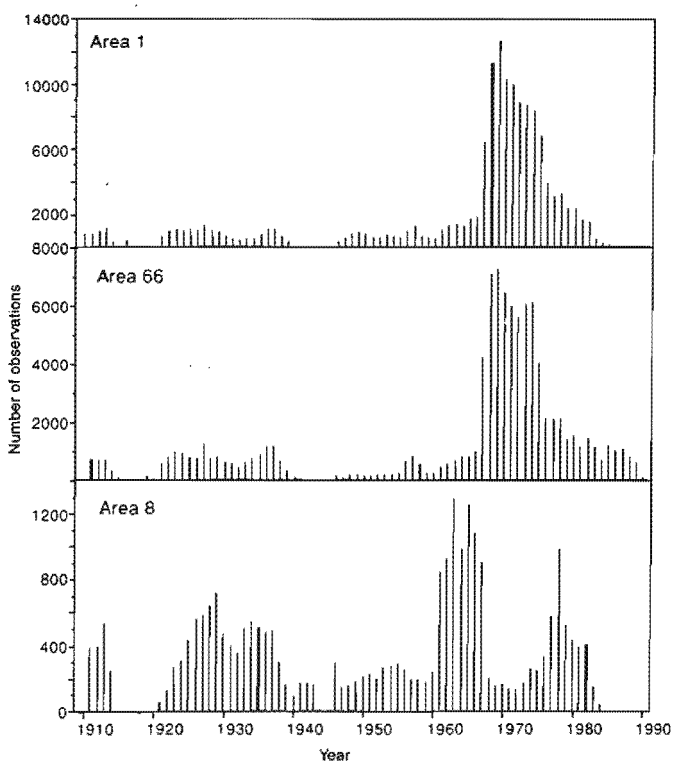

Fig. 2. Numbers of SST records available for (*a*) area 1, (*b*) area 66 and (*c*) area 8, January 1910–December 1990. Locations of the areas are shown in Fig. 1.

Then, the 'distance' between areas i and j was computed over all pairs of values e_{it} and e_{jt} as:

$$d_{ij} = \left(\sum_{t} \frac{(e_{it} - e_{jt})^2}{n_{ij}} \right)^{\frac{1}{2}} \qquad (2)$$

where n_{ij} was the number of months for which both the residuals e_{it} and e_{jt} were available.

The 88 × 88 matrix of distances between areas thus computed was represented in three dimensions using non-metric ordination.[22] The output from a non-metric ordination can be read in the same way as a geographical map. Areas are plotted close together in the three-dimensional space if they have similar patterns for their residuals. Thus a group of areas plotted close together must show cohesion in their SST patterns through time. The quality of the output from a non-metric ordination is measured by means of a stress function, and the algorithm attempts to find the representation with minimum stress.[22] The stress function used was equation 5.3.6 of Greenacre and Underhill.[23] This function does not suffer from the disadvantages of the standard Kruskal-Shepard stress function,[24] in that with the modified stress function the detailed local arrangement of the points is meaningful and can be interpreted.[23]

Results

Table 2 shows, by block, the percentage variation in the data which is explained by the model based on a Fourier-type regression [(Equation (1)]. For the southernmost areas (82–88; 40°–50°S), only a small proportion of the variance (0–15%) was accounted for, indicating a poor fit of the model. For areas 71–81, between 35° and 40°S, the percentage explained improved to between 39 and 75%. For areas farther north (1–70), the model accounted for more than 70% of the observed variance in 63 out of 70 instances, and for more than 60% of the variation in five additional cases. The two exceptions were areas 55 (52%) and 6, where only 25.4% of the variance was modelled. In five cases (areas 14, 25, 34, 35 and 44) the model described more than 90% of the variation.

Monthly SST values computed by the Fourier-type regression model are shown in Fig. 1. As expected, temperatures are higher near the Equator and decrease with increasing latitude. South of 40°S, where the model fits poorly, the seasonal signal is reduced and the seasonal pattern often unexpected, perhaps due to the unpredicted movement of all the major oceanographic currents that converge in that area. For example, the Fourier model computes maxima for areas 86 and 87 in June and July respectively, during the austral winter.

For all areas in the region bounded by 25°S and 40°S the maximum monthly SST is predicted for February, as it is also in subtropical latitudes off Namibia and in the Indian Ocean. Farther to the north and west the maxima occur in March. In the extreme northwest (0–15°S, 10–25°W) and in the extreme northeast (0–5°S, 40–50°E) the maxima are in April. In area 4 the maximum is in May.

North of 40°S, modelled monthly minima in SST occur in August or September in all areas, except area 4 (October) and area 7 (July). In all 38 areas of the Atlantic Ocean west of 10°E, south of 5°S and north of 40°S minima occur in September, except in area 16, at the extreme northeast of this region, where the predicted minimum is in August. In five of these areas, the predicted value for August is as low as that for September. In area 75, southwest of the continent, the minimum is also in September, as it is in areas 80 and 81, at the southeast of the region considered. Elsewhere in the Indian Ocean, around the southern rim of Africa, along the west coast of the continent and in most of the areas in the Atlantic Ocean immediately south of the Equator, the minimum occurs in August.

The seasonal signal has the highest amplitude off northern Namibia and Angola (areas 17 and 27) (Fig. 1). In area 27 the difference between the maximum and minimum is 7.1°C. The amplitude in the seasonal signal decreases from Namibia south along the African west coast, but at the southern rim of Africa increases again. The amplitude tends to decrease away from coastal areas in the Atlantic Ocean. However, there is a pronounced seasonal signal in the southwest of the region considered (e.g. areas 49, 50, 60 and 61). In the Indian Ocean, the amplitude in the seasonal signal decreases from south to north.

The coefficient for the long-term trend [(b in Equation (1)] was positive for 73 areas and negative for just 15 (Table 3), indicating a predominant tendency to warming. Five of the areas with long-term cooling were south of Africa; the 10 others were all in the Atlantic Ocean. In a possible scenario of global warming, the values of the coefficient b were such that, extrapolating over the 81-year period (1910–1990), the predicted increase in SST ranged from 0.1 to 2.2°C. The extreme values are due mostly to errors of extrapolation from observation periods in some areas being concentrated into periods much shorter than 81 years. The average increase in sea surface temperature shown by the model is 0.46°C, excluding area 6 and all areas south of 40°S. When only those areas for which the trend contributed significantly are considered, the average increase in sea surface temperature shown by the model is 0.63°C.

The representation of the coherence between residuals obtained for different areas is shown in Fig. 3, in which the third (vertical) dimension is reflected by the size of the squares repre-

Table 2. Percentage variation in the data explained by the Fourier-type regression model for each area. Also shown are months in which the predicted maximum and minimum SSTs will occur.

Area	% variation explained	Month of predicted Maximum	Minimum	Area	% variation explained	Month of predicted Maximum	Minimum
1	73.4	April	August	45	63.7	February	August
2	79.7	April	August	46	85.5	February	August
3	78.9	March–April	August	47	77.6	February	August
4	87.8	May	October	48	80.9	February	August
5	87.2	March	August	49	80.4	February	Aug.–Sept.
6	25.4	March	August	50	79.0	February	Aug-Sept.
7	81.6	March	July	51	85.3	February	September
8	77.4	April	August	52	84.0	February	September
9	76.1	April	August	53	89.2	February	September
10	69.7	April	September	54	87.2	February	Aug.–Sept.
11	75.5	April	September	55	52.0	February	August
12	76.8	April	September	56	87.9	February	August
13	87.4	March–April	Aug.–Sept.	57	83.0	February	August
14	90.2	March–April	September	58	80.5	February	August
15	82.1	March	September	59	74.6	February	August
16	84.5	March	August	60	73.3	February	September
17	81.3	March	August	61	76.3	February	September
18	86.0	March	August	62	83.8	February	September
19	84.3	March	August	63	84.8	February	September
20	65.8	April	September	64	89.6	February	August
21	66.4	April	September	65	69.8	Jan.–Feb.	August
22	76.9	April	September	66	79.9	Jan.–Feb.	August
23	81.6	March	September	67	63.7	February	August
24	88.2	March	September	68	82.7	February	August
25	90.7	March	September	69	70.8	February	August
26	86.1	March	September	70	71.9	February	August
27	74.2	March	August	71	57.7	February	September
28	86.7	March	August	72	49.2	February	September
29	75.0	March	August	73	50.3	February	September
30	67.6	March	Aug.–Sept.	74	40.7	February	September
31	80.4	March	September	75	38.7	February	September
32	82.1	March	September	76	74.5	February	August
33	84.2	March	September	77	74.2	February	August
34	91.5	March	September	78	47.7	February	Aug.–Sept.
35	91.4	March	September	79	49.7	Feb.–Mar.	Aug.–Sept.
36	72.8	March	August	80	53.8	March	September
37	84.7	March	August	81	59.4	February	September
38	86.0	March	August	82	4.5	May–June	September
39	75.3	March	August	83	3.5	May–June	October
40	69.3	March	Aug.–Sept.	84	0.5	May–June	September
41	79.2	March	September	85	13.9	June	December
42	85.0	March	September	86	0.1	July	December
43	85.7	March	September	87	1.4	February	November
44	91.8	March	September	88	4.3	February	September

Table 3. Long-term trend coefficients (slopes) for each area. Also shown is the significance (* $P < 0.05$, ** $P < 0.01$, *** $P < 0.005$, **** $P < 0.001$) and the change in sea surface temperature (°C) predicted by the model over the total period of study (1910 to 1990).

Area	Coefficient	Significance	Long-term change (°C)	Area	Coefficient	Significance	Long-term change (°C)
1	−0.0008		−0.059	45	0.0300	****	2.220
2	−0.0008		−0.059	46	0.0114	****	0.844
3	0.0012		0.148	47	0.0077	****	0.570
4	0.0010		0.074	48	0.0026		0.192
5	0.0030	**	0.222	49	0.0020		0.148
6	−0.1090	****	−8.066	50	0.0088	****	0.651
7	−0.0053	***	−0.392	51	0.0068	****	0.503
8	0.0060	****	0.444	52	0.0041	**	0.303
9	0.0059	****	0.437	53	0.0013		0.096
10	0.0067	****	0.496	54	0.0019		0.141
11	0.0012		0.089	55	0.0150	****	1.110
12	0.0026	*	0.192	56	0.0103	****	0.762
13	0.0016		0.118	57	0.0090	****	0.666
14	−0.0010		−0.074	58	0.0095	****	0.703
15	0.0048	***	0.355	59	0.0161	****	1.914
16	−0.0074	****	−0.548	60	−0.0021		−0.155
17	0.0044	*	0.326	61	0.0071	**	0.525
18	0.0058	****	0.429	62	0.0022		0.163
19	0.0060	****	0.444	63	0.0053	***	0.392
20	0.0065	****	0.481	64	0.0035		0.259
21	0.0056	****	0.414	65	0.0110	****	0.814
22	0.0051	****	0.377	66	0.0063	****	0.466
23	0.0052	****	0.385	67	0.0112	****	0.829
24	0.0045	****	0.333	68	0.0008		0.059
25	0.0010		0.074	69	0.0057	***	0.422
26	0.0125	****	0.925	70	0.0000		0.000
27	0.0072	***	0.533	71	0.0157	****	1.162
28	0.0062	****	0.459	72	0.0180	****	1.332
29	0.0074	****	0.548	73	0.0227	****	1.680
30	−0.0034	*	0.252	74	0.0104		0.770
31	0.0060	****	0.444	75	−0.0087		−0.644
32	0.0074	****	0.548	76	0.0075	****	0.555
33	0.0001		0.074	77	−0.0045	**	−0.333
34	0.0046	****	0.340	78	0.0263	****	1.946
35	0.0008		0.059	79	0.0231	****	1.709
36	0.0000		0.000	80	0.0128	****	0.947
37	0.0112	****	0.829	81	0.0140	****	1.036
38	0.0066	****	0.488	82	0.0222	*	1.643
39	0.0090	****	0.666	83	0.0006		0.044
40	−0.0019		−0.363	84	-0.0133		−0.984
41	0.0067	****	0.496	85	0.0141		1.043
42	−0.0021		−0.155	86	0.0484	****	3.582
43	0.0050	****	0.370	87	−0.0365	****	−2.701
44	0.0022	*	0.163	88	−0.0071		−0.525

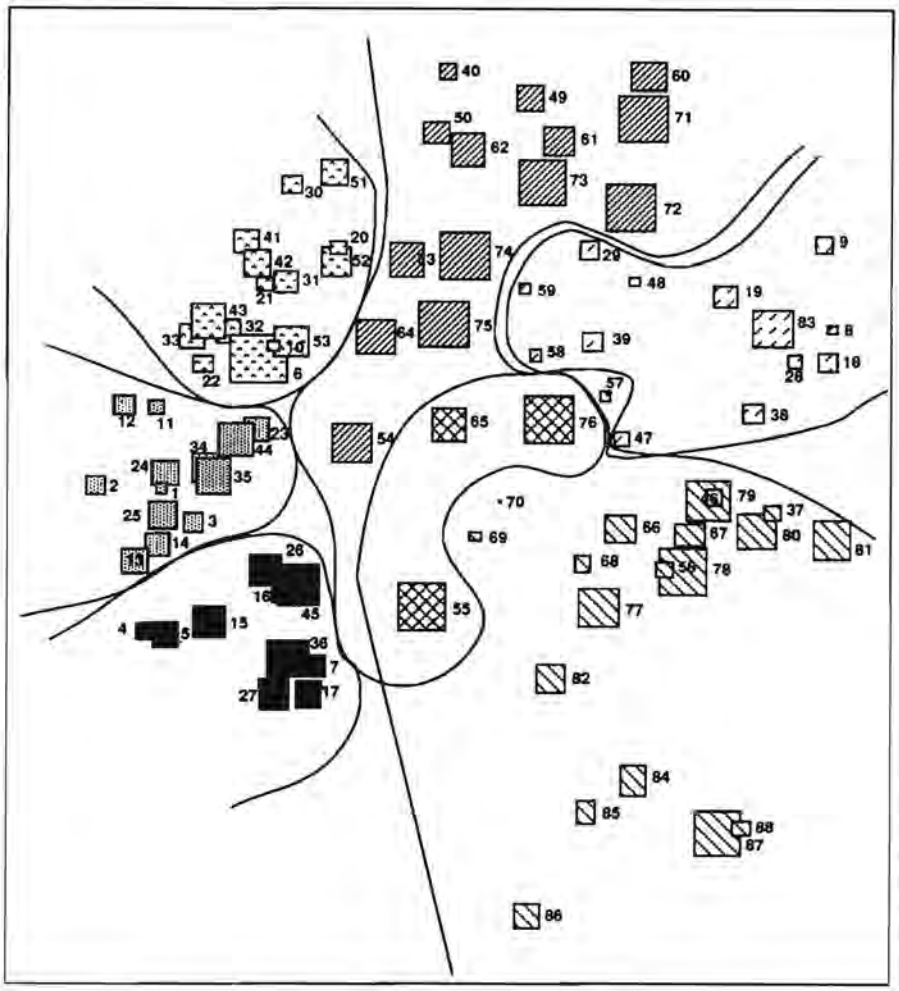

Fig. 3. Three-dimensional representation of coherence between residuals obtained for different areas. Residuals were determined as the difference between observed and modelled SST values. The vertical dimension is indicated by the size of the square. In the two-dimensional plane, six groups of areas may be distinguished, as indicated by the shading.

senting areas. Squares of equal size fall on the same plane. In dimensions 1 and 2, the areas group approximately into six categories (Fig. 3). These generally conform with integral areas of the ocean (Fig. 4). One group represents most of the Indian Ocean between the Equator and 30°S. A second includes areas in the Indian Ocean along the southeast African coast, extending into the South Atlantic Ocean. Four groups fall in the Atlantic Ocean, orientated mainly in a northwest–southeast direction.

In the third dimension, four groups of areas can be discerned (Fig. 5). Two of these, at more or less the same plane, represent areas in the Indian Ocean and at the northwest of that portion of the Atlantic Ocean considered (Fig. 6). One includes many of the areas located between 35° and 40°S. The fourth group includes areas in the southeast Atlantic Ocean, north of 35°S, as well as most of the areas south of 40°S.

Discussion

The Fourier-type regression model does not adequately fit data for areas south of 40°S, where density of data is sparse (Table 1) and annual patterning is not strong. Elsewhere, the model accounts for much of the variation in data, except for area 6 (Table 2). In general, for areas north of 40°S, months predicted for maximum and minimum temperatures agree with the analysis of Bottomley *et al.*,[25] who used data for the period 1951–1980 from the Meteorological Office's Main Marine Data Bank augmented by other sources. In the case of maximum temperatures, the same month was predicted for 71 of the 81 areas north of 40°S, whereas for seven others there was a difference of only one pentad (five days) from the month predicted by our model. For minimum temperatures, there was agreement in 67 instances and a difference of one pentad in eight others. For both maximum and minimum temperatures, there was only one instance (area 4) in which the month predicted differed by more than two pentads from the analysis of Bottomley *et al.*[25]

The warmest SSTs between 25 and 40°S are predicted by the Fourier-type model to occur in February, lagging the austral solstice by about two months. North of about the Tropic of Capricorn, the maximum is predicted for March or later, at the conclusion of the period during which the sun is south of the Equator. The maxima in April to the northwest and northeast of the region studied may result from westward advection of warm surface waters by the South Equatorial Currents of the Atlantic and Indian oceans, respectively.

Minima in the south-west Indian Ocean north of 35°S and along the west coast of Africa are generally in August, whereas minima farther west in the Atlantic Ocean, except immediately south of the Equator, are usually in September. The shape of the seasonal SST curve in the Indian Ocean is approximately sinusoidal, roughly tracking the seasonal insolation curve, whereas in several Atlantic areas the seasonal SST curve has a 'saw tooth' configuration. The reasons for these differences between the Atlantic and Indian oceans are not obvious, although differences in cloud cover may be a contributory factor. Cloud cover during much of the year in the south-west Indian Ocean north of 35°S is typically less than 40% and in the south-east Atlantic and south of Africa between 35° and 40°S it is typically greater than 50%.[26] However, Gorshkov[26] shows that the contributions of high level (highly reflective) clouds to these percentages are not resolved.

The pronounced seasonal signals off Angola and along the

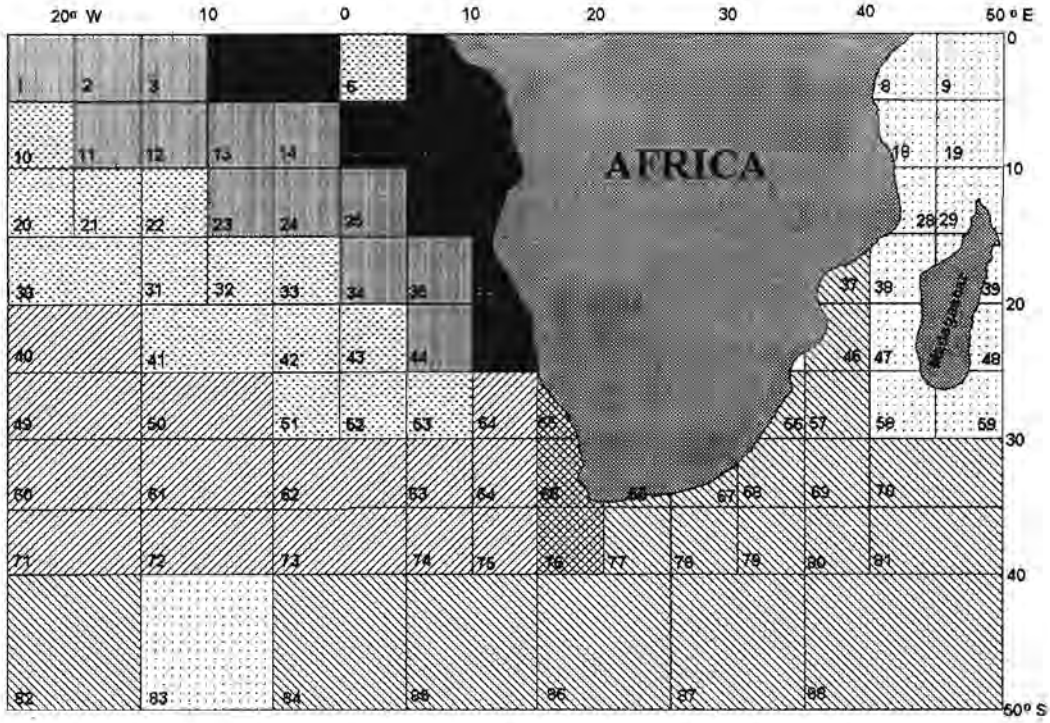

Fig. 4. Locations of six groups of areas apparent from coherence in the two-dimensional plane of Fig. 3.

southern rim of Africa correspond respectively with the Angola Current and the western extremity of the Agulhas Current. The rapid drop in SST along the Angolan coast after March is caused by seasonal upwelling.[27] Off Durban (area 56), SST in the Agulhas Current region is some 4°C cooler in winter than in summer.[28] The change in the temperature of the Agulhas Current is likely to account for at least part of the enhanced seasonal signal south of Africa.

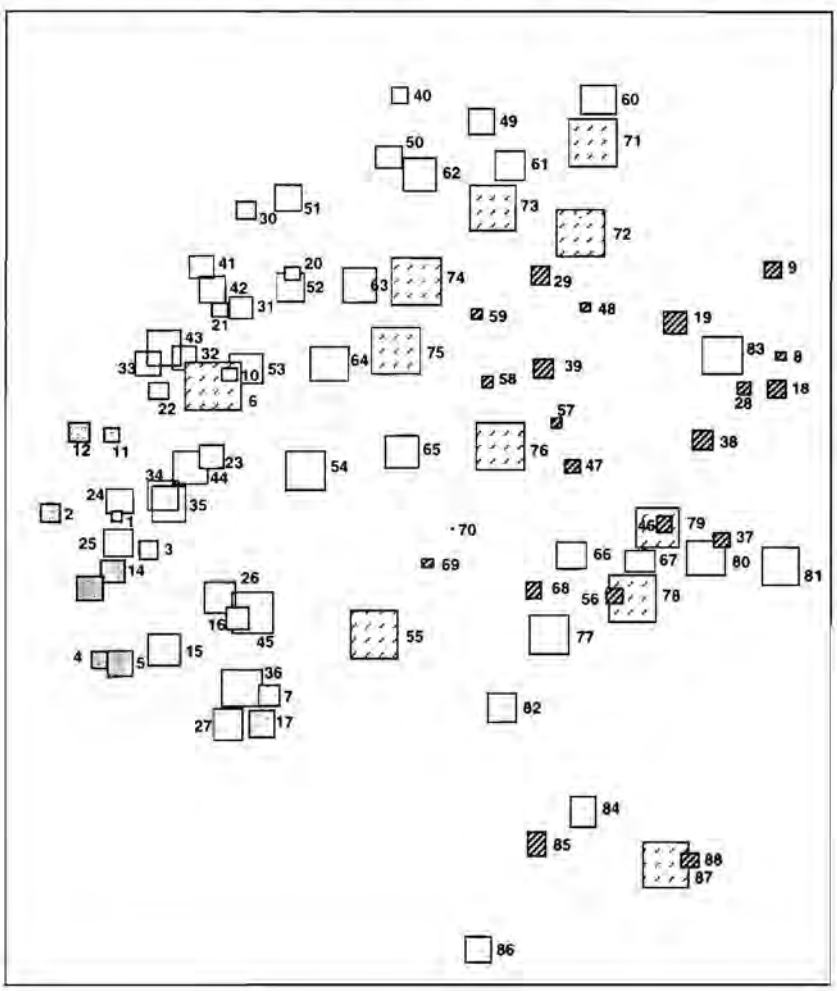

Fig. 5. The four groups of areas (shaded) that may be distinguished from the vertical dimension of the three-dimensional representation of coherence between areas. The vertical dimension is indicated by the relative size of the squares.

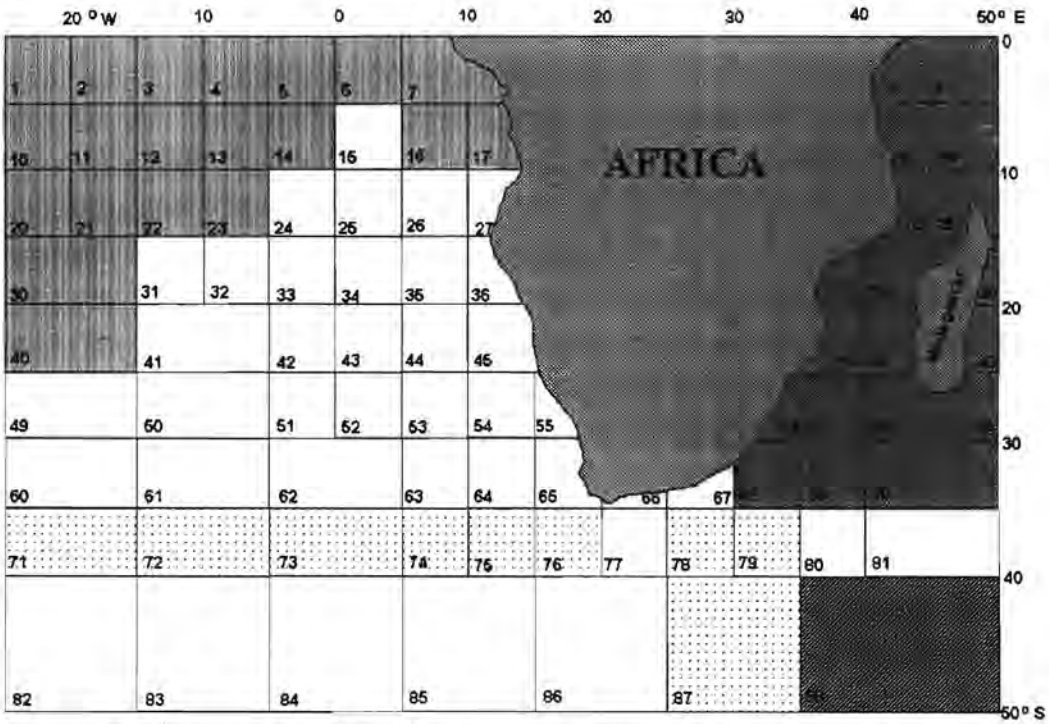

Fig. 6. Locations of four groups of areas apparent from coherence in the vertical plane of Fig. 5.

A pronounced seasonal signal in the central South Atlantic immediately north of the Subtropical Convergence (STC), namely, in areas 49, 50, 60 and 61, is apparent in Fig. 1. A contributing factor is likely to be relatively free meridional seasonal migration of surface isohalines in the area. Reference to Gorshkov[26] and other climatic atlases, however, shows that surface isotherms in the western and central sectors of the South Atlantic tend to migrate meridionally seasonally through more than 10° of latitude. In contrast the surface isohalines are relatively static. It is also worth noting that the water boundary (STC) and the wind boundary (maximum convergence of Ekman drift) are nearly coincident south of the Brazil and Agulhas currents,[29] but near 15°W their separation is at its maximum in the South Atlantic. Together with the relatively shallow but pronounced summer thermocline in the area near 15°W, this may explain the large seasonal SST signal in the central South Atlantic. The STC in the South Atlantic west of about 0° has a very different structure from the STC south of Africa and in the southwest Indian Ocean, where the Agulhas Current and its retroflection is a dominant feature, with consequent local intensification of the STC as a front and reduced seasonal meridional movement of the isotherms.

In both the two-dimensional plane and the vertical dimension, areas in the northern sector of that portion of the Indian Ocean considered are grouped together (Figs 4 and 6). The vertical dimension places areas at the northwest of that section of the Atlantic Ocean investigated at a similar level to areas in the Indian Ocean (Fig. 5). However, these two groups are separated in the two-dimensional plane.

In the two-dimensional plane, there is coherence between areas along the southeastern coast of Africa, extending to the southwest of Africa (Fig. 4). These areas correspond to the region of influence of the Agulhas Current, its retroflection zone and the Agulhas Return Current.[28]

The two-dimensional plane distinguishes four sectors of the Atlantic Ocean between the Equator and 40°S (Fig. 4). In the northeast are a group of squares that correspond to the warm water regimes of the Angola Current and the South Equatorial Counter Current system. This group of squares also includes the waters off Namibia, which along the coast form part of the cool Benguela upwelling system.[30] Most data used in the analysis were collected along the main shipping route between South Africa and Europe, offshore of the cool coastal upwelling area. To the southwest of these areas lies a group of areas that corresponds with the South East Trade Wind drift and the South Equatorial Current in the South Atlantic.[28] Farther southwest is another group of squares corresponding with water in the south central Atlantic Ocean. Lastly, there is a group of areas associated with or north of the Subtropical Convergence. This group of areas extends north between 5° and 25°W, approximating a northern location of the Subtropical Convergence.[28]

In the vertical dimension of the representation of coherence between SST residuals, there is also indication of separation of the waters of the Subtropical Convergence in the Atlantic Ocean, between 35° and 40°S (Fig. 6.), from those immediately north of it. The vertical dimension distinguishes a group of areas off southwest Africa extending to the southwest. These areas represent northeasterly flow of water from the southwest associated with the anticyclonic gyre in the South Atlantic.[28]

The poor fit of the Fourier-type regression model to the data for areas 82–88 and 6 means that residuals for these areas will approximate the original (unmodelled) data. This resulted in these areas being computed by Equation (2) as having relatively large distances from the remaining areas, but nonetheless fairly close to each other. The multidimensional scaling algorithm locates areas 82–88 (except 83) as a group outside of the main cluster of points (Fig. 3). The positioning of area 6 is anomalous, and is related to the poor fit of the seasonal model for this area. The raw SST data for this area were checked. No obvious errors were located, but the reason for the poor fit needs further investigation. These areas aside, the three-dimensional representation appears to capture adequately many of the known features of the physical environment that may be expected to influence SST.

What emerges from the analysis is that the coastal marine

environment off southwestern Africa has associations with many different oceanographic regimes. Especially areas 55, 65 and 76, at the centre of the representation of coherence between SST residuals, appear to have affinities with many groups of areas. They are likely to be influenced from the north, west, south and east, and hence to be highly variable. This will complicate prediction of change in the environment, and hence in the distributions and abundances of fish and other marine organisms that are influenced by environmental change. Other coastal areas around subequatorial Africa are not subject to as many diverse influences. Hence their marine environment may be more predictable.

The scope of the analysis does not permit investigation of linkages between the North and South Atlantic — the area of investigation was bounded to the north by the Equator. However, coherence of SST residuals in the Atlantic Ocean near the equator and farther south along the African coast accords with the possibility that some signals in the marine environment may propagate over long distances in this region. Similar coherence in SST residuals in other parts of the oceans investigated indicates that such remote forcing of the marine environment may be widespread. A next step will be to investigate more closely the data points that give rise to the coherence, to ascertain whether specific events can be recognized that are responsible for the observed patterns.

Although prediction of change in the marine environment off southern Africa remains complex, it is clear that well-defined seasonal patterns in SST exist in most of the areas investigated. These should facilitate prediction of the seasonal occurrence of migratory animals with temperature preferences, e.g. some tunas.[31] In most regions around subequatorial Africa there appears to have been warming of surface waters between 1910 and 1990, the average increase being 0.46°C. This is less than seasonal fluctuations in SST, but may still have an influence on the fauna. Continued warming could see an expansion of the distributions of tropical species. Bottomley *et al.*[25] record a long-term warming of SST in both the South Atlantic and South Indian oceans, as well as globally, since 1860, with periods of increased temperature being interspaced with dips. In both the South Atlantic and South Indian oceans they illustrate a warming of about 0.6°C between 1910 and 1990, in agreement with the Fourier-type model for areas where the trend was significant.

We thank Neville Paynter of Ematek for his invaluable help during the downloading of all data. Thanks also go to Ian Hunter (Maritime Office; Weather Bureau) for supplying SST charts. L.G. Underhill received support from the Foundation for Research Development and the University of Cape Town Research Committee, and C.A. Villacastín-Herrero from the FRD and Benguela Ecology Programme. We also gratefully acknowledge the comments of an anonymous referee.

Received 18 April 1995; accepted 15 January 1996.

1. Shannon L.V., Crawford R.J.M., Pollock D.E., Hutchings L., Boyd A.J., Taunton-Clark J., Badenhorst A., Mellville-Smith R., Augustyn A.J., Cochrane K.L., Hampton I., Nelson G., Japp D.W. and Tarr R.J.Q. (1992). The 1980s — a decade of change in the Benguela ecosystem. *S. Afr. J. mar. Sci.* **12**, 271–296.
2. Shannon L.V., Boyd A.J., Brundrit G.B. and Taunton-Clark J. (1986). On the existence of an El Ninõ-type phenomenon in the Benguela system. *J. mar. Res.* **44**, 495–520.
3. Shannon L.V., Agenbag J.J., Walker N.D. and Lutjeharms J.R.E. (1990). A large-scale perspective on interannual variability in the environment in the South-East Atlantic. *S. Afr. J. mar. Sci.* **9**, 161–168.
4. Crawford R.J.M., Siegfried W.R., Shannon L.V., Villacastín-Herrero C.A. and Underhill L.G. (1990). Environmental influences on marine biota off southern Africa. *S. Afr. J. Sci.* **86**, 330–339.
5. Duncombe Rae C.M., Boyd A.J. and Crawford R.J.M. (1992). 'Predation' of anchovy by an Agulhas ring: a possible contributory cause of the very poor year-class of 1989. *S. Afr. J. mar. Sci.* **12**, 167–173.
6. Crawford R.J.M., Underhill L.G., Shannon L.V., Lluch-Belda D., Siegfried W.R. and Villacastín-Herrero C.A. (1991). An empirical investigation of trans-oceanic linkages between areas of high abundance of sardine. In *Long-term Variability of Pelagic Fish Populations and Their Environment*, eds T. Kawasaki, S. Tanaka, Y. Toba and A. Taniguchi, pp. 319–332. Pergamon, Oxford.
7. Crawford R.J.M. and Shannon L.V. (1988). Long-term changes in the distribution of fish catches in the Benguela. In *Long-term Changes in Marine Fish Populations*, eds T. Wyatt, and M.G. Larrañeta, pp. 449–480. Instituto de Investigaciones Marinas de Vigo, Vigo.
8. Lluch-Belda D., Crawford R.J.M., Kawasaki T., MacCall A.D., Parrish R.H., Schwartzlose R.A. and Smith P.E. (1989). World-wide fluctuations of sardine and anchovy stocks: the regime problem. *S. Afr. J. mar. Sci.* **8**, 195–205.
9. Lluch-Belda D., Schwartzlose R.A., Serra R., Parrish R.H., Kawasaki T., Hedgecock D. and Crawford R.J.M. (1992). Sardine and anchovy regime fluctuations of abundance in four regions of the world oceans: a workshop report. *Fish. Oceanogr.* **1**, 339–347.
10. McLain D.R., Brainard R.E. and Norton J.G. (1985). Anomalous warm events in eastern boundary current systems. *Rep. Calif. coop. oceanic Fish. Invest.* **26**, 51–64.
11. Walker N.D. (1987) Interannual sea surface temperature variability and associated atmospheric forcing within the Benguela system. In *The Benguela and Comparable Ecosystems*, eds A.I.L. Payne J.A. Gullard and K.H. Brink. *S. Afr. J. mar. Sci.* **5**, 121–132.
12. Brundrit G.B. (1984). Monthly sea level variability along the west coast of southern Africa. *S. Afr. J. mar. Sci.* **2**, 195–203.
13. Bruce J.G. (1987). XBT observations between 10°N-10°S in the Atlantic from ships of opportunity, complemented by a XBT survey. *Woods Hole Oceanographic Inst. Tech. Rep.* WHOI-87-41, 373 pp.
14. Folland C.K. and Hsiung J. (1986). Correction of seasonally-varying biases in uninsulated bucket sea surface temperature data using a physical model. *Met. Office Synoptic Climatology Branch Memo*, 154.
15. Saur J.F.T. (1963). A study of the quality of sea water temperatures reported in logs of ships' weather observations. *J. appl. Meteorol.* **2**, 417–425.
16. Barnett T.P. (1984). Long-term trends in surface temperature over the ocean. *Mon. Weath. Rev.* **112**, 303–312.
17. Folland C.K. and Parker D.E. (1988). Comparison of corrected sea surface and air temperature for the globe and the hemispheres, 1856–1988. In *Proc. 13th Annual Climate Diagnostics Workshop*. U.S. Dept. of Commerce, 160–165.
18. Jones P.D., Wigley T.M.L. and Wright P.B. (1986). Global temperature variations between 1861 and 1984. *Nature* **322**, 430–434.
19. Folland C.K., Parker D.E. and Kates F.E. (1984). Worldwide marine temperature fluctuations 1856–1981. *Nature* **310**, 670–673.
20. Zucchini W. and Adamson P.T. (1984). The occurrence and severity of droughts in South Africa. *WRC Report 91/1/84*. Water Research Commission, Pretoria.
21. Underhill L.G., Prys-Jones R.P., Harrison J.A. and Martinez P. (1992). Seasonal patterns of occurrence of Palaeoarctic migrants in southern Africa using atlas data. *Ibis* **134**, Suppl. 1, 99–108.
22. Kruskal J.B. (1964). Multidimensional scaling by optimizing goodness of fit to a nonmetric hypothesis. *Psychometrika* **29**, 1–27.
23. Greenacre M.J. and Underhill L.G. (1981). Scaling a data matrix in a low-dimensional Euclidean space. In *Topics in Applied Multivariate Analysis*, ed. D.M. Hawkins, pp. 183–268. Cambridge University Press, Cambridge.
24. Kruskal J.B. (1977). The relationship between multidimensional scaling and clustering. In *Classification and Clustering*, ed. J. Van Ryzin, pp. 17–43, Academic Press, New York.
25. Bottomley M., Folland C.K., Hsiung J., Newell R.E. and Parker D.E. (1990). *Global Ocean Surface Temperature Atlas*. Meterological Office, Bracknell, U.K.
26. Gorshkov S.G. (1978). *World Ocean Atlas*, vol. 2. *Atlantic and Indian Oceans*. Pergamon, Oxford.
27. Boyd A.J., Salat J. and Masó M. (1987). The seasonal intrusion of relatively saline water on the shelf off northern and central Namibia. In *The Benguela and Comparable Ecosystems*, eds A.I.L. Payne, J.A. Gullard and K.H. Brink. *S. Afr. J. mar. Sci.* **5**, 107–120.
28. Shannon L.V. (1989). The physical environment. In *Oceans of Life off Southern Africa*, eds A.I.L. Payne and R.J.M. Crawford, pp. 12–27. Vlaeberg, Cape Town.
29. Deacon G.E.R. (1982). Physical and biological zonation in the Southern Ocean. *Deep-Sea Res.* **29**, 1–15.
30. Shannon L.V. (1985). The Benguela ecosystem part I. Evolution of the Benguela, physical features and processes. *Oceanogr. Mar. Biol. Ann. Rev.* **23**, 105–182.
31. Shannon L.V., Van der Elst R.P. and Crawford R.J.M. (1989). Tunas, bonitos, Spanish mackerels and billfish. In *Oceans of Life off Southern Africa*, edit. A.I.L. Payne and R.J.M. Crawford, pp. 188–197. Vlaeberg, Cape Town.